



Effects of minor Sc addition on the microstructure and mechanical properties of 7055 Al alloy during aging

G.B. Teng^a, C.Y. Liu^{a,b,*}, Z.Y. Ma^{b,**}, W.B. Zhou^c, L.L. Wei^a, Y. Chen^a, J. Li^c, Y.F. Mo^c

^a Key Laboratory of New Processing Technology for Nonferrous Metal & Materials, Ministry of Education, Guilin University of Technology, Guilin 541004, China

^b Shenyang National Laboratory for Materials Science, Institute of Metal Research, Chinese Academy of Sciences, 72 Wenhua Road, Shenyang 110016, China

^c Alnan Aluminium Co., Ltd., Nanning 530000, China



ARTICLE INFO

Keywords:

Al alloy

Microstructure

Mechanical properties

ABSTRACT

This study investigated the effects of 0.25% (mass ratio) Sc addition on the microstructure and mechanical properties of 7055 alloy during aging. Sc addition induced a grain boundary effect, which refined the grains of the 7055 alloy. Sc addition also increased the precipitation nucleation efficiency and promoted the uniform precipitation of the η' phase of 7055 alloy during aging. Compared with pure 7055 alloy, 7055 alloy with Sc exhibited improved hardness, tensile strength, ductility, and thermal stability. This improvement was attributed to the finer size, higher density, more uniformly distributed η' phase, less η phase, and finer Al grains of 7055 alloy with Sc compared with those of 7055 alloy without Sc.

1. Introduction

Al–Zn–Mg–Cu series (7xxx) alloys are widely used in the aeronautics and astronautics industries because of their ultra-high strength and fracture toughness [1–5]. Recent advancements of aerospace technologies have required the fabrication of 7xxx alloys with better mechanical properties and thermal stability.

These 7xxx alloys typically refer to age-hardened Al alloys, and the mechanical properties of these alloys are mainly determined by precipitation characteristics, such as composition, size, and distribution [6–9]. Thus, the mechanical properties of the 7xxx alloys can be effectively improved by developing strategies for controlling precipitation.

Numerous studies have investigated the effects of Sc and Zr on the microstructure and mechanical properties of 7xxx alloys [10–12]. The primary $\text{Al}_3(\text{Sc,Zr})$ phase can serve as a heterogeneous nucleation site for Al grains during solidification, leading to grain refinement in 7xxx alloys [10]. Moreover, $\text{Al}_3(\text{Sc,Zr})$ precipitates obtained by homogenization can inhibit the recrystallization and grain coarsening that occur during subsequent deformations and heat treatments because of the grain boundary (GB) pinning effect induced by the $\text{Al}_3(\text{Sc,Zr})$ phase [13–16]. Therefore, compared with conventional 7xxx alloys, 7xxx alloys with Sc and Zr exhibit improved mechanical properties due to the grain refinements. However, limited studies have explored the effects of

Sc and Zr additions on the precipitation behavior of 7xxx alloys during artificial aging.

Chen et al. [13,14] and Jiang et al. [15,16] recently found that a minor addition of the rare earth element Sc into an Al–Cu alloy affected the precipitation behavior of the alloy during artificial aging. The Sc atoms segregated at the θ' matrix interfaces and inhibited the growth of the θ' phase or the transformation of the θ' phase into θ phase. Compared with the Al–Cu alloy, the Al–Cu–Sc alloy exhibited higher strength under similar aging conditions because of the higher precipitation strengthening of the latter. Therefore, Sc addition is expected to optimize the precipitation behavior of 7xxx alloys.

In this study, 7055 and 7055 with 0.25% (mass ratio) Sc (7055–0.25Sc) alloys were artificially aged at 120 °C for different times to understand the effects of minor Sc addition on the precipitation behavior and resultant mechanical properties of 7xxx alloys. In addition, a higher aging temperature of 150 °C was implemented to examine the effect of Sc addition on the thermal stability of 7xxx alloys.

2. Experimental methods

Rolled 7055 and 7055–0.25Sc alloy sheets (rolling temperature was 470 °C, and rolling reduction was 70%) were used as raw materials. The chemical compositions of these two alloys are presented in Table 1. The sheets were subjected to solution treatment at 470 °C for 2 h, water

* Corresponding author at: Key Laboratory of New Processing Technology for Nonferrous Metal & Materials, Ministry of Education, Guilin University of Technology, Guilin 541004, China.

** Corresponding author.

E-mail addresses: lcy261@glut.edu.cn (C.Y. Liu), zym@imr.ac.cn (Z.Y. Ma).

<https://doi.org/10.1016/j.msea.2017.12.067>

Received 2 July 2017; Received in revised form 19 November 2017; Accepted 15 December 2017

Available online 16 December 2017

0921-5093/ © 2017 Elsevier B.V. All rights reserved.

Table 1
Chemical composition of the 7055 and 7055–0.25Sc alloys.

	Zn	Mg	Cu	Zr	Sc
7055	7.82	1.95	2.24	0.16	–
7055–0.25Sc	7.81	1.93	2.24	0.16	0.25

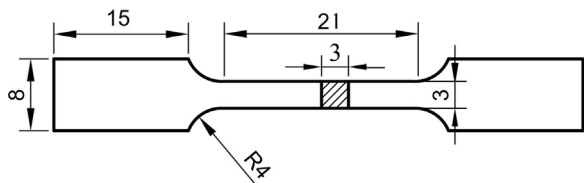


Fig. 1. Schematic of the tensile specimen (mm).

quenched, and then aged at 120 °C and 150 °C from 1 h to 72 h.

The microstructures of the alloys were examined by optical microscopy (OM) and transmission electron microscopy (TEM). Prior to TEM analysis, the films were grinded to a thickness of 50 μm and then thinned with a twinjet electropolishing device. Hardness was measured with a Vickers microhardness tester. The tensile tests were conducted on an Instron-3369-type testing machine at a strain rate of $4 \times 10^{-4} \text{ s}^{-1}$. The tensile specimens were machined parallel to the rolling direction. Fig. 1 shows the dimensions and shape of the tensile specimens.

3. Results

Fig. 2 shows the micrographs of the 7055 and 7055–0.25Sc alloys after solution treatment. The average sizes of the grains along the short dimension in the as-rolled 7055 and 7055–0.25Sc alloys were approximately 30 (Fig. 2a) and 10 μm (Fig. 2b), respectively. Equiaxed 20–30 nm particles were observed in the 7055 alloy (Fig. 2c). The selected diffraction area (SAD), the chemical composition and the heat treatment process suggested that these particles constituted the Al_3Zr phase with face centered cubic (fcc) structure [17]. A considerably

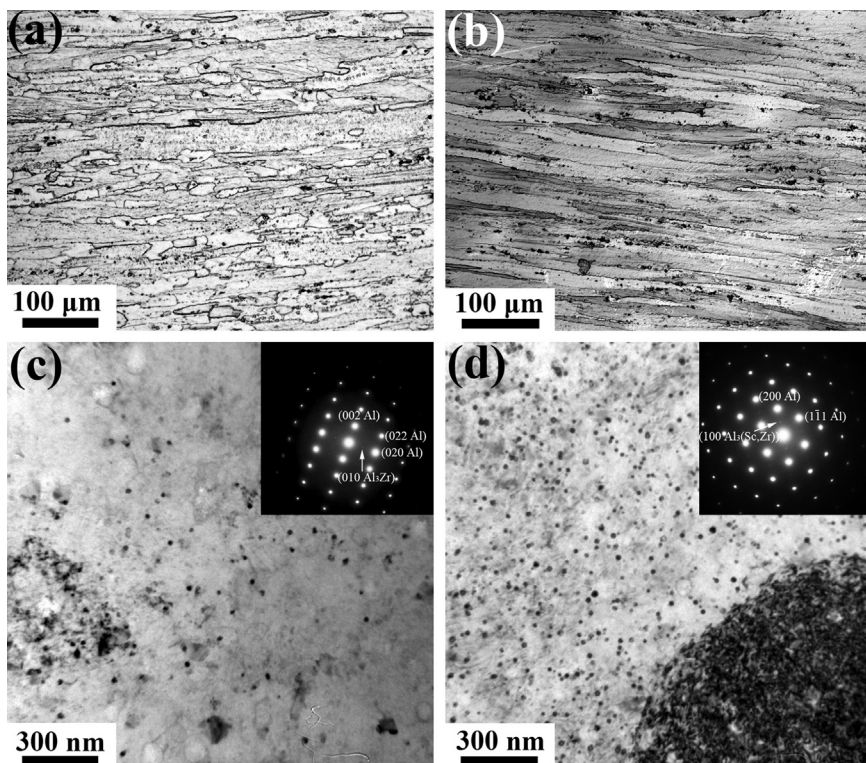


Fig. 2. OM micrographs of the (a) 7055 and (b) 7055–0.25Sc alloys. TEM micrographs of the (c) 7055 and (d) 7055–0.25Sc alloys after solution treatment.

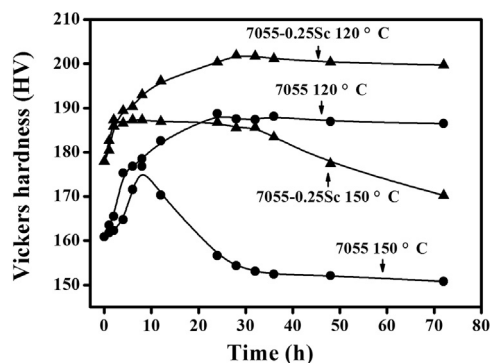


Fig. 3. Variation of Vickers hardness with aging time of the 7055 and 7055–0.25Sc alloys at different temperatures.

higher density of nano-sized particles was observed in the 7055–0.25Sc alloy, and some of these particles were located at the GBs (Fig. 2d). The SAD, the chemical composition, and the heat treatment process indicated the nano-sized particles in the 7055–0.25Sc alloy after solution treatment constituted the $\text{Al}_3(\text{Sc,Zr})$ phase with face centered cubic (fcc) structure.

Fig. 3 shows the age-hardening curves of the 7055 and 7055–0.25Sc alloys during aging. The 7055 and 7055–0.25Sc alloys exhibited a hardening behavior, and the peak-aged times of these two alloys were in the range of 24–26 h during aging at 120 °C. The peak-aged times of the 7055 and 7055–0.25Sc alloys were reduced to 8 and 5 h, respectively, when the aging temperature was increased to 150 °C. The hardness value of the 7055–0.25Sc alloy was higher than that of the 7055 alloy for each aging parameter. Furthermore, the 7055–0.25Sc alloy maintained its high hardness for 30 h of aging at 150 °C. By contrast, the 7055 alloy exhibited a significantly shorter high-hardness duration, and the hardness rapidly decreased after the peak value was reached. Thus, Sc addition increased the thermal stability of the 7055 alloy during high-temperature aging. Moreover, the peak hardness values of both alloys at a lower aging temperature of 120 °C were

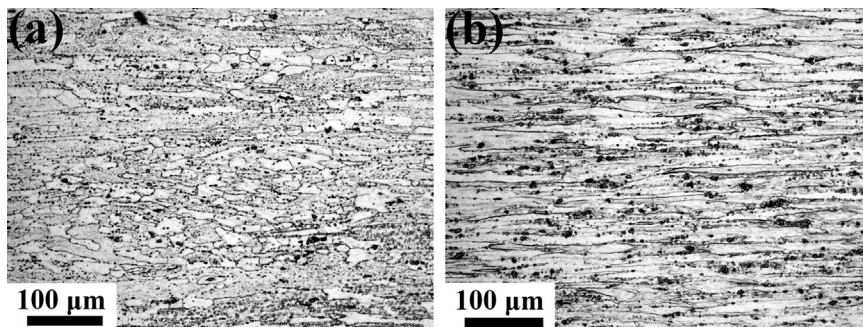


Fig. 4. OM micrographs of the (a) 7055 and (b) 7055–0.25Sc alloys after aging at 150 °C for 30 h.

considerably higher than those at a higher temperature of 150 °C.

Fig. 4 shows the OM micrographs of the 7055 and 7055–0.25Sc alloys after 30 h of aging at 150 °C (over-aged condition). The grain size and structure of the over-aged samples were insignificantly changed compared with those of the solution-treated samples (Fig. 2a and b).

Fig. 5 shows the TEM micrographs of the 7055 alloys after aging under different conditions. For the samples aged at 120 °C, a high density of precipitates with size of several nanometers was observed in the grain interior, whereas large-size precipitates were discontinuously distributed along the GBs after 12 h of aging (Fig. 5a and b). When the aging time was prolonged to 24 h, the precipitated phase coarsened in the grain interior, and the number density of the particles with size larger than 50 nm was approximately $9 \times 10^{13} \text{ m}^{-3}$. The selected diffraction area revealed that the nanoparticles in the grain interior contained η' precipitates and Al_3Zr phases (Fig. 5c). The large-size phase was discontinuously distributed along the GBs, and precipitate free zones (PFZ) were observed in the sample (Fig. 5d). The density of particles with size larger than 50 nm in the 150 °C/8 h 7055 alloy was approximately $2 \times 10^{14} \text{ m}^{-3}$, which was slightly higher than that of 120 °C/24 h 7055 alloy (Fig. 5e and f). When the aging time was further increased to 30 h at 150 °C, the precipitated phase further coarsened (Fig. 5g), and the dark-field image excited by the reflection of η phase demonstrated that a high density of plate- or rod-shaped equilibrium η phase was observed in the grain interior of the 150 °C/30 h 7055 alloy (Fig. 5h).

Fig. 6 shows the TEM micrographs of 7055–0.25Sc alloys after aging under different conditions. Compared with the 120 °C/12 h 7055 alloy, the 7055–0.25Sc alloy under the same aging condition presented finer precipitates in the grain interior and no large-size precipitates along the GBs (Fig. 6a and b). Moreover, a high density of fish-eye-like $\text{Al}_3(\text{Sc,Zr})$ particles, which were identified by SAD, were observed in the sample, and some of the particles were located at the dislocations near the GBs, as shown by the arrows in Fig. 6b. The 120 °C/24 h and 150 °C/8 h 7055–0.25Sc samples displayed similar microstructures, and exhibited lower density of large-size precipitates than the 7055 alloy under the same aging conditions (Fig. 6c–f). $\text{Al}_3(\text{Sc,Zr})$ particles were also observed at the dislocations near the GBs, as shown by the arrows in Fig. 6d and f. Precipitates with sizes of up to 60 nm were observed in the 150 °C/30 h 7055–0.25Sc alloy. However, compared with the 150 °C/30 h 7055 alloy, this sample exhibited a considerably lower density of large-size precipitates (Fig. 6g). Plate- or rod-shaped η phase particles were observed near the $\text{Al}_3(\text{Sc,Zr})$ particles in the 150 °C/30 h 7055–0.25Sc alloy, as shown by the arrows in Fig. 6h.

Fig. 7 shows the stress–strain curves of the 7055 and 7055–0.25Sc alloys after aging under different conditions. The mechanical properties of the two alloys are provided in Table 2. The 7055–0.25Sc alloys exhibited better mechanical properties than those of the 7055 alloys under the same aging condition. Compared with the 120 °C/24 h samples, the 150 °C/8 h samples presented lower ultimate tensile strength (UTS) and elongation (EL). The strength of the 150 °C/30 h 7055 alloy was obviously lower than that of the 150 °C/30 h 7055 alloy, and the 7055–0.25Sc alloy maintained a high strength up to 30 h of aging. The

120 °C/24 h 7055–0.25Sc alloy demonstrated the best mechanical properties, with a yield strength (YS), UTS, and EL of up to 600, 679 MPa, and 14%, respectively.

4. Discussion

Precipitation strengthening was the most significant strengthening mechanism in the 7xxx alloys after aging treatment. The precipitation sequence of the 7xxx alloys was described as: supersaturated solid solution \rightarrow GP zones \rightarrow metastable η' phase \rightarrow stable η phase; the η' phase acted as the main strengthening phase in these alloys [17].

For the 7055 alloy, the quenching-induced grain interior defects, such as dislocations and vacancies, were annihilated during artificial aging. Thus, only the GBs provided preferential nucleation sites for the precipitates. The precipitates first precipitated at the GBs, continued to grow, and then transformed into a stable phase by absorbing solute atoms surrounding them in the grain interior [18–20]. Then, the nucleation of the precipitates near the GBs was inhibited, and the PFZ was formed (Fig. 5).

For the 7055–0.25Sc alloy, the movements and annihilations of the quenching-induced crystal defects were suppressed during aging because of the pinning effect of the $\text{Al}_3(\text{Sc,Zr})$ particles (Fig. 6b, d, and f), and additional nucleation sites were available for precipitates in the 7055–0.25Sc alloy. Thus, a significant amount of precipitates was observed near the $\text{Al}_3(\text{Sc,Zr})$ particles in the 150 °C/30 h 7055–0.25Sc alloy (Fig. 6h). The high efficiency of precipitation nucleation decreased the density of the η phase along the GBs in the 7055–0.25Sc alloy, and no obvious PFZ was observed in this alloy after aging.

In addition, more Zn and Mg atoms were consumed in the Al lattice, and the formation of the η phase and the growth of η' precipitates were suppressed during the further because of the high efficiency of precipitation nucleation in the 7055–0.25Sc alloy. Thus, compared with the 7055 alloy, the 7055–0.25Sc alloy exhibited a lower density of the large η phase and a finer size of the η' phase under the same aging conditions (Figs. 5 and 6).

The superior hardness and thermal stability of the 7055–0.25Sc alloy during aging (Fig. 3) was attributed to the following factors. First, the 7055–0.25Sc alloy had a smaller grain size than that of the 7055 alloy under the same aging conditions (Figs. 2 and 4) because the nano-sized $\text{Al}_3(\text{Sc,Zr})$ precipitates pinned the GBs and retained more fine grains during heat treatments [14–16,21]. Consequently, the 7055–0.25Sc alloy exhibited a higher GB strengthening. Second, the size, density, and distribution of the η' phase in the 120 °C/24 h and 150 °C/8 h 7055 samples were optimized by the minor Sc addition. Moreover, minor Sc addition prevented the η' phase from coarsening and transforming into the η phase in the 7055 alloy during aging. Consequently, the 7055–0.25Sc alloy exhibited a higher precipitation strengthening.

The higher GB and precipitation strengthening provided the 7055–0.25Sc alloys with a higher tensile strength than that of the 7055 alloys. The higher thermal stability of the 7055–0.25Sc alloy during aging at 150 °C was attributed to the precipitation inhibition effects,

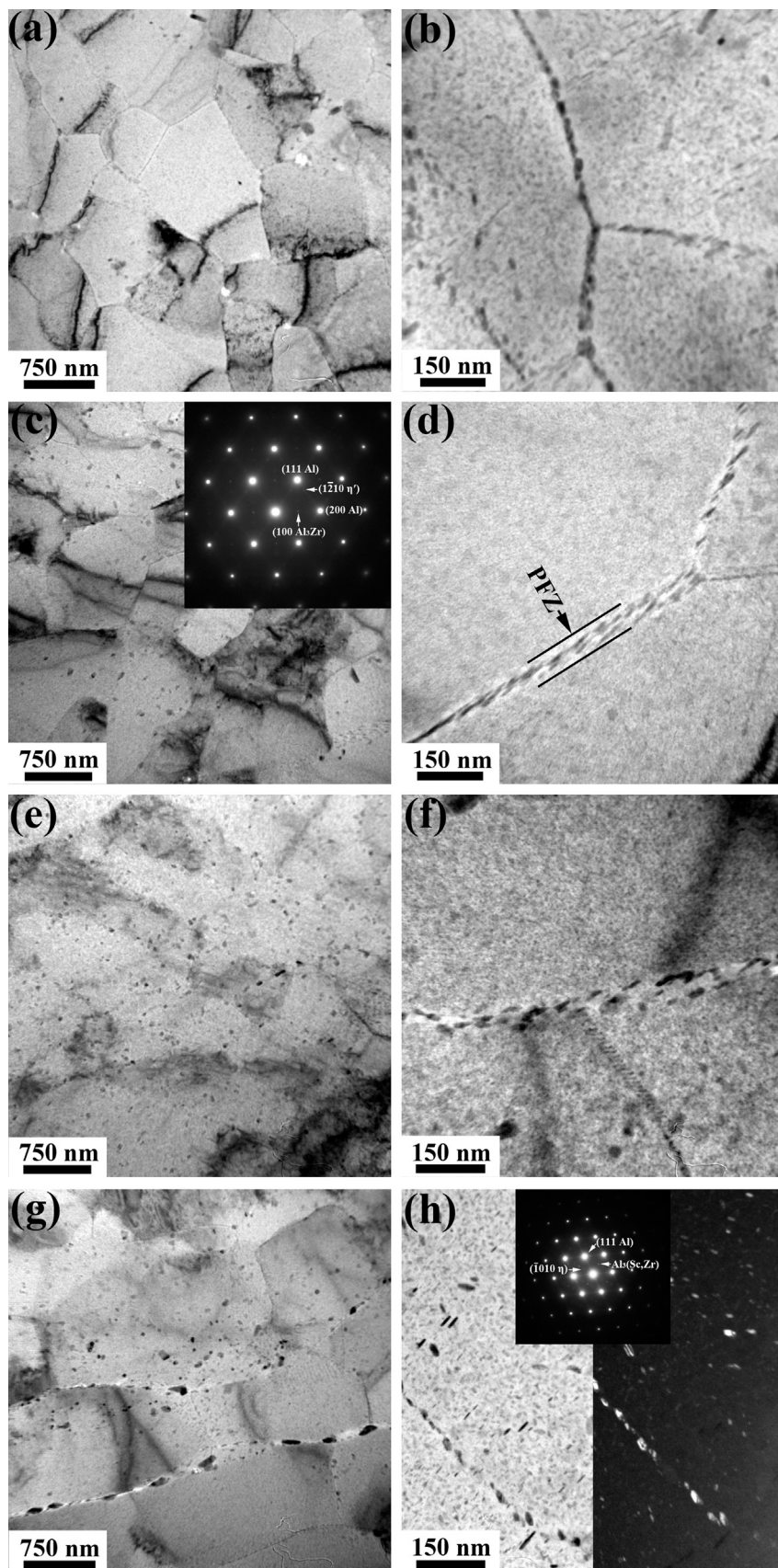


Fig. 5. TEM micrographs of the 7055 alloys aged at (a and b) 120 °C for 12 h (120 °C/12 h), (c and d) 120 °C for 24 h (120 °C/24 h), (e and f) 150 °C for 8 h (150 °C/8 h), and (g and h) 150 °C for 30 h (150 °C/30 h).

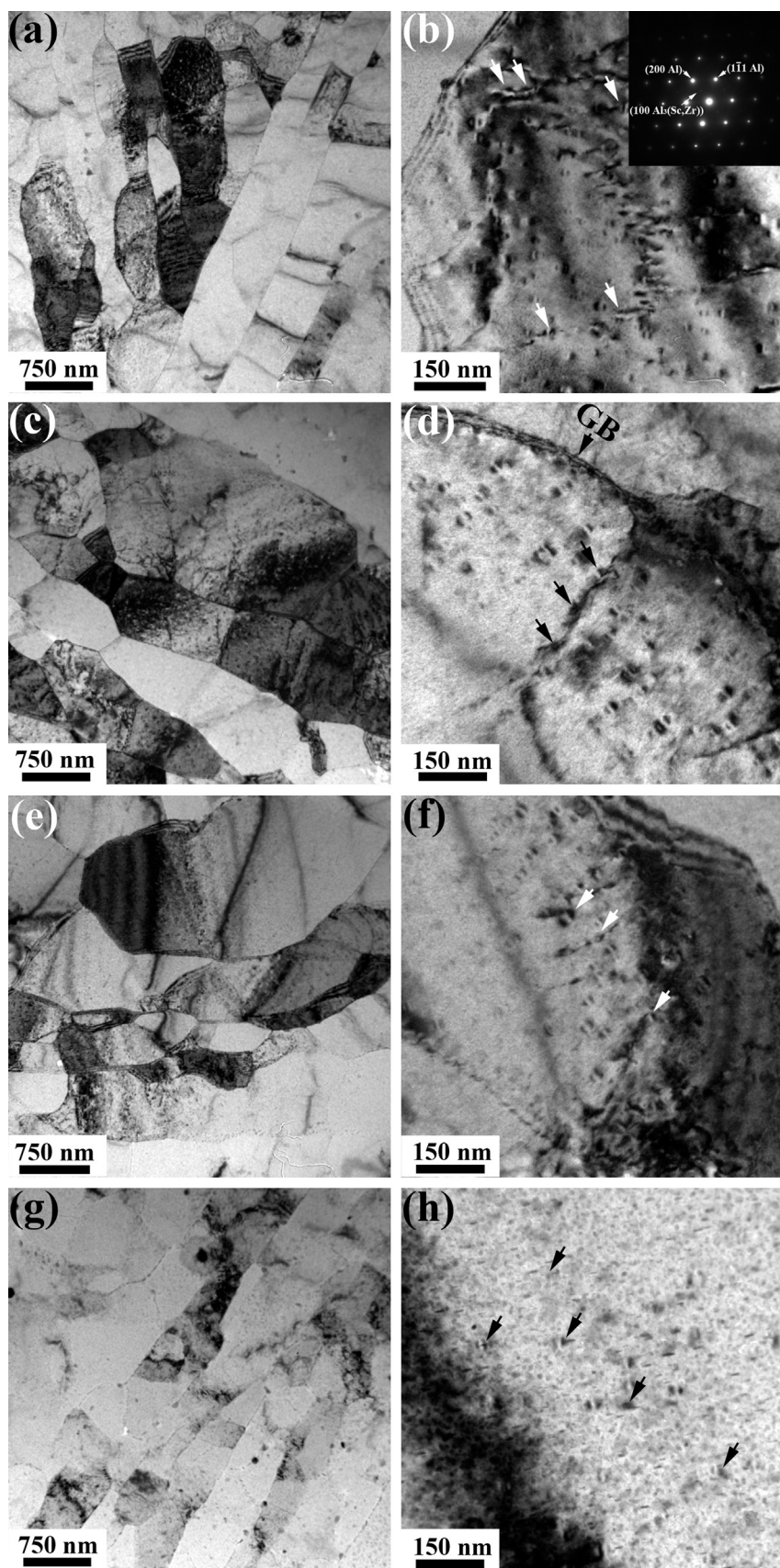


Fig. 6. TEM micrographs of the 7055–0.25Sc alloys aged at (a and b) 120 °C for 12 h (120 °C/12 h), (c and d) 120 °C for 24 h (120 °C/24 h), (e and f) 150 °C for 8 h (150 °C/8 h), and (g and h) 150 °C for 30 h (150 °C/30 h). The arrows in (b), (d), (f), and (h) denote the $Al_3(Sc, Zr)$ phase.

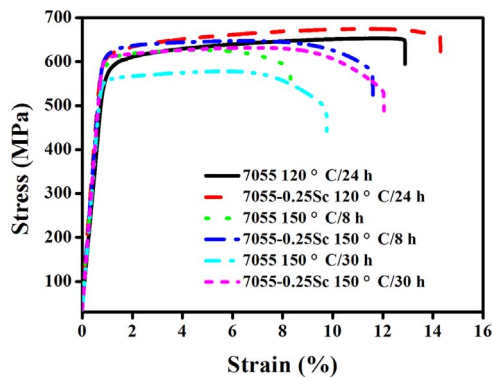


Fig. 7. Stress–strain curves of the aged 7055 and 7055–0.25Sc alloys.

Table 2

Tensile properties of the 7055 and 7055–0.25Sc alloys with various aging parameters.

		YS (MPa)	UTS (MPa)	EL (%)
120 °C/24 h	7055	577	654	13
	7055–0.25Sc	600	679	14
150 °C/8 h	7055	589	627	8
	7055–0.25Sc	611	648	12
150 °C/30 h	7055	557	585	10
	7055–0.25Sc	602	628	12

including the coarsening of the metastable phase and its transformation stable phase, induced by the Sc addition.

Compared with the 7055 alloys, the 7055–0.25Sc alloys exhibited higher EL. Minor Sc addition exerted two positive effects on the ductility of the 7055 alloy. First, the $\text{Al}_3(\text{Sc,Zr})$ particles pinned the GBs of the Al alloys during deformation and subsequent solution treatments [22,23]. Thus, the grain sizes of the 7055–0.25Sc alloy were lower than those of the 7055 alloy (Figs. 2 and 4). The fine grain structure contributed to a higher ductility, because the strain localization was prevented by the redistribution of the stresses during tension. Thus, considerable elongation was achieved before failure. Second, the GBs and dislocations were pinned by the $\text{Al}_3(\text{Sc,Zr})$ particles, and the accumulation of the dislocations was delayed during tensile test, thus the crack growth of the 7055–0.25Sc alloy was inhibited.

Compared with the 120 °C/24 h samples, the 150 °C/8 h samples exhibited lower hardness, UTS, and EL. The higher density of the large η precipitates in the 150 °C/8 h samples was responsible for the lower precipitation strengthening, which in turn resulted in reduced hardness and strength. Zhao et al. [24] found that nano-sized precipitates contributed to the accumulation of dislocations in Al alloys during tension, thereby increasing the work hardening rate and improving the ductility of Al alloys. In the present study, the 120 °C/24 h samples exhibited a higher work hardening rate than the 150 °C/8 h samples sample because of the finer precipitates (Fig. 7). Therefore, the 120 °C/24 h samples achieved a higher EL.

5. Conclusions

The effects of minor Sc addition on the precipitation behavior and

resultant mechanical properties of the 7055 alloy during aging were investigated. The following conclusions were drawn:

- (1) Sc addition refined the grains of the 7055 alloy because of the GB pinning effect of the nano-sized $\text{Al}_3(\text{Sc,Zr})$ phase.
- (2) Sc addition increased the hardness and thermal stability of the 7055 alloy during aging.
- (3) Sc addition promoted the uniform precipitation of the η' phase, inhibited the coarsening of the η' phase, and prevents its transformation into η phase in the 7055 alloy.
- (4) Sc addition improved the mechanical properties, such as strength and ductility, of the 7055 alloy after aging. This phenomenon was mainly attributed to the grain refinement, finer size, higher density, more uniformly distributed η' phase, and less η phase in the 7055–0.25Sc alloys.

Acknowledgements

This work was funded by the National Natural Science Foundation of China (No.51601045), the Guangxi “Bagui” Teams for Innovation and Research, and the Research Program of Science and Technology of Guangxi (No. GKAB16380021).

References

- [1] J.R. Zuo, L.G. Hou, J.T. Shi, H. Cui, L.Z. Zhuang, J.S. Zhang, *J. Alloy. Compd.* 716 (2017) 220–230.
- [2] L.L. Wei, Q.L. Pan, H.F. Huang, L. Feng, Y.L. Wang, *Int. J. Fatigue* 66 (2014) 55–64.
- [3] C. Mondal, A.K. Mukhopadhyay, T. Raghu, V.K. Varma, *Mater. Sci. Eng. A* 454 (2007) 673–678.
- [4] J.C. Williams, J.E.A. Starke, *Acta Mater.* 51 (2003) 5775–5799.
- [5] S.D. Liu, Y. Zhang, W.J. Liu, Y.L. Deng, X.M. Zhang, *Trans. Nonferrous Met. Soc. China* 20 (2010) 1–6.
- [6] L.M. Wu, M. Seyring, M. Rettenmayr, W.H. Wang, *Mater. Sci. Eng. A* 527 (2010) 1068–1073.
- [7] Y. Liu, S. Liang, D.M. Jiang, *J. Alloy. Compd.* 689 (2016) 632–640.
- [8] Y.Q. Xu, L.H. Zhan, S.J. Li, X.T. Wu, *Rare Metal. Mater. Eng.* 46 (2017) 0355–0362.
- [9] X.Y. Peng, Q. Guo, X.P. Liang, Y. Deng, Y. Gu, G.F. Xu, Z.M. Yin, *Mater. Sci. Eng. A* 688 (2017) 146–154.
- [10] B. Li, Q.L. Pan, X. Huang, Z.M. Yin, *Mater. Sci. Eng. A* 616 (2014) 219–228.
- [11] M. Zhang, T. Liu, C.N. He, J. Ding, E.Z. Liu, C.S. Shi, J.J. Li, N.Q. Zhao, *J. Alloy. Compd.* 658 (2016) 946–951.
- [12] Y. Deng, Z.M. Yin, J.Q. Duan, K. Zhao, B. Tang, Z.B. He, *J. Alloy. Compd.* 517 (2012) 118–126.
- [13] B.A. Chen, G. Liu, R.H. Wang, J.Y. Zhang, L. Jiang, J.J. Song, J. Sun, *Acta Mater.* 61 (2013) 1676–1690.
- [14] B.A. Chen, L. Pan, R.H. Wang, G. Liu, P.M. Cheng, L. Xiao, J. Sun, *Mater. Sci. Eng. A* 530 (2011) 607–617.
- [15] L. Jiang, J.K. Li, P.M. Cheng, G. Liu, R.H. Wang, B.A. Chen, J.Y. Zhang, J. Sun, M.X. Yang, G. Yang, *Mater. Sci. Eng. A* 607 (2014) 596–604.
- [16] L. Jiang, J.K. Li, G. Liu, R.H. Wang, B.A. Chen, J.Y. Zhang, J. Sun, M.X. Yang, G. Yang, J. Yang, X.Z. Cao, *Mater. Sci. Eng. A* 637 (2015) 139–154.
- [17] G.S. Peng, K.H. Chen, S.Y. Chen, H.C. Fang, *Mater. Sci. Eng. A* 528 (2011) 4014–4018.
- [18] D. Wang, D.R. Ni, Z.Y. Ma, *Mater. Sci. Eng. A* 494 (2008) 360–366.
- [19] D. Wang, Z.Y. Ma, Z.M. Gao, *Mater. Chem. Phys.* 117 (2009) 228–233.
- [20] D. Wang, Z.Y. Ma, *J. Alloy. Compd.* 469 (2009) 445–450.
- [21] S.D. Liu, X.M. Zhang, M.A. Chen, J.H. You, *Mater. Charact.* 59 (2008) 53–60.
- [22] H.F. Huang, F. Jiang, J. Zhou, L.L. Wei, M.C. Zhong, X.T. Liu, *J. Alloy. Compd.* 644 (2015) 862–872.
- [23] F.C. Liu, Z.Y. Ma, F.C. Zhang, *J. Mater. Sci. Technol.* 28 (2012) 1025–1030.
- [24] Y.H. Zhao, X.Z. Liao, S. Cheng, E. Ma, Y.T. Zhu, *Adv. Mater.* 18 (2006) 2280–2283.